Calcium Induced Shrinking of NaPA Chains: A SANS Investigation of Single Chain Behavior

Ralf Schweins,[†,‡] Peter Lindner,[‡] and Klaus Huber*[,†]

Fakultät für Naturwissenschaften, Department Chemie, Universität Paderborn, Warburger Strasse 100, D-33098 Paderborn FRG

Received June 6, 2003; Revised Manuscript Received October 6, 2003

ABSTRACT: Calcium ions were used to induce a shrinking process with sodium polyacrylate coils in aqueous 0.01 M NaCl. By means of light scattering, four solutions with promising intermediates were selected for a detailed investigation by small-angle neutron scattering. All intermediates were half as large in size as the corresponding unperturbed dimensions but still had radii of gyration that were 45% larger than the hydrodynamic radius. The resulting SANS curves showed power laws typical for objects with a sharp boundary. They were compared with various model curves. From these models, a mixture of spheres and dumbbells resulted in theoretical curves that agreed best with experiments. The sphere size of single spheres and spheres in dumbbells was roughly 10 nm. Two spheres on a dumbbell had an averaged distance larger by almost an order of magnitude. The results are considered to be compatible with pearl necklace-like transition states of shrinking polyelectrolyte chains.

Introduction

Water very often is a poor solvent for neutral organic polyacids. Deprotonation turns the polyacids into polyelectrolytes. Now, solution behavior is dominated by electrostatic forces and the chains become highly soluble in water. These electrostatic forces by far exceed conventional excluded volume interactions observed with neutral polymers. In salt-free water, polyelectrolyte dimensions are highly expanded, although still far from adopting a rigid rodlike shape.[1,2] If an alkaline salt like NaCl is added, the strong electrostatic interactions are increasingly screened and the expanded polyelctrolyte coils start to shrink. The shrinking process may even lead to unperturbed dimensions if the concentration of alkaline salt is high enough.[3−5] Beyond this alkaline salt level, phase separation usually sets in.[6−8] The latter phenomena has been denoted as salting out of polyelectrolytes or, alternatively, as H-type precipitation because the concentration of alkaline salt is high and independent of the polymer concentration.[8] In this case, the effect of the added salt is nonspecific and governed by its electric charges. Such salts are denoted as inert salts in the present paper.

If salts of bivalent cations are used instead of an inert salt, coil shrinking and precipitation of the same polyelectrolytes were often observed at much lower salt concentrations. In this case, phase separation is denoted as L-type precipitation.[8−10] As could be shown for polyacrylates, the amount of alkaline earth cations required for a precipitation increases with increasing polyanion content, being roughly equimolar to the carboxylate residues. Obviously, alkaline earth cations are chemical entities that form complex bonds with the anionic carboxylate residues along the polyelectrolyte backbone, thus interacting more specifically than alkaline cations do. Addition of an inert salt shifts this phase boundary toward larger values of bivalent metal cation concentration. Thus, an increasing content of an inert salt gradually replaces the specifically interacting alkaline earth cations via ion exchange.

Phase transition in polymer solutions is by no means restricted to polyelectrolyte precipitation. In the case of neutral polymers, it is induced by a temperature shift that modifies inter- and intramolecular interactions. If the concentration of neutral macromolecules is low enough, phase separation is kinetically suppressed and changes are restricted to intramolecular interactions. The intramoleculer interactions lead to a collapse of the neutral polymers, which finally adopt a sphere-like shape.[11−15] The collapse is caused by quenching polymer solutions from the Θ temperature, where the chains adopt their unperturbed dimensions, to just below its separation threshold. First time-resolved experiments by means of dynamic light scattering on the collapse mechanism revealed a two-stage kinetics with a crumpled globule in the first stage, which finally collapsed further to a compact globule or sphere. The time regime for the induced collapse was on the order of a few minutes and required extremely skillfull experiments.[16]

In the field of polyelectrolytes, such a collapse of chains has been clearly demonstrated for the system sodium polyacrylate (NaPA) as it approaches the phase boundary of an L-type precipitation induced by Ca^{2+} ions.[17]

Theoretical consideration on polyelectrolyte collapse began with the publications by Khokhlov,[18] Kantor and Kardar,[19,20] and Rubinstein et al.[21] As in any theory on polyelectrolyte solutions, the counterions and the ions of added low molecular weight salts were treated as elementary electric charges or multiples thereof with a finite size and without any additional chemical feature. Therefore, they can only account for nonspecific counterion condensation. For bad solvent conditions, calculations[18−21] led to the widely accepted picture of a cascade of transitions that includes a pearl necklace-like structure.[19−24] The underlying physics is the shape instability of charged droplets which can be influenced by the solvent condition and the charge density.

* To whom correspondence should be addressed. E-mail: huber@chemie.uni-paderborn.de.
[†] Universität Paderborn.
[‡] Institut Laue-Langevin, Large Scale Structures Group, B.P. 156, 6, rue Jules Horowitz, F-38042 Grenoble Cedex 9, France.

10.1021/ma0347722 CCC: $25.00
Published on Web 11/20/2003

Further aspects of this collapse process investigated theoretically or by computer simulation were the impact of polyelectrolyte concentration[25] and solvent condition,[24,25] the influence of an added inert salt,[26] the valency of counterions,[27] the impact of chain stiffness on the collapse,[28] the coexistence of both monovalent and multivalent cations,[28,29] and the degree of ionization of the polyelectrolyte chain.[30] Recently, even the dynamics of the collapse process was investigated as depending on the valency of the counterions, solvent quality, and shape of the counterions.[31] This offers the chance to compare the dynamics of the collapse process of polyelectrolytes with that of neutral chains.[32,33] Interestingly, pearl necklace shapes were also predicted for the latter process.[32,33]

Meanwhile, first experimental indications for pearl necklace-like intermediates of collapsing polyelectrolyte chains have appeared in the literature. Essafi et al.[34] discussed the existence of extended hydrophobic domains in solutions of highly charged polyelectrolytes with a hydrophobic backbone on the basis of small-angle X-ray scattering (SAXS) and fluorescence emission from semidilute solution of poly(styrenesulfonate) (PSS). Further evidence for dense hydrophobic PSS domains was presented later by Williams et al.,[35,36] who extended the former SAXS experiments on the same system. This evidence was deduced from a gradual decrease of the exponent of the power law $q^* \sim c^{\alpha}$ relating the location q^* of a characteristic scattering peak to the PSS concentration c. The decrease of the exponent within $0.5 < \alpha < 0.33$ was generated by lowering the effective charge fraction f of the corresponding PSS chains. Ellipsometry and atomic force microscopy (AFM) on PSS layers adsorbed from the very solutions on an appropriate substrate were in support of such pearl-like PSS domains. Geissler et al.[37] induced the shrinking of a polycation in salt-free water by addition of acetone and performed small-angle neutron scattering (SANS) experiments with collapsed chains. By comparing the overall size of the polycations with the behavior of the scattering curves at high q values, they found an indication for a string of three to four pearls. Similar to this type of shrinking, Morawetz et al.[38] generated solutions of NaPSS, NaPA, and sodium polymethacrylate (NaPMA) close to the phase boundary by adding methanol to aqueous solutions and performed NMR spectroscopy. They found a reduction of the ^{1}H signals that was attributed to the loss of mobile segments. According to Morawetz et al.,[38] those segments were used to form the pearls. The most recent investigation also seems to provide the most direct indication for pearl necklace structures, although not performed in solution. Minko et al.[39] succeeded in producing AFM images that demonstrate a cascade of structural transitions of poly(2-vinylpyridine) induced by Pd^{2+} complexation. The cascade started with worm-like chains and finally led to pearl necklace-like structures.

Further insight into the impact of multivalent counterions was presented by Dubois and Boué[40] on the conformation of PSS chains and by Francois et al.[41,42] and by Sabbagh et al.[43] on the conformation of acrylate chains.

Dubois and Boué[40] added Ca^{2+} and La^{3+} ions to semidilute solutions of PSS chains and characterized the chain conformation by means of SANS experiments based on the zero-averaged contrast technique. A deviation from the shape of a worm-like chain was observed with an increasing amount of added cations. At the same time, the chains increased their effective mass per unit length. The changes may result in part from intermolecular bridging supported in semidilute solutions. Francois et al. performed X-ray scattering on poly(methacrylic acid) and partly neutralized PMA in water.[41] Scattering curves of PMA at low pH suggested a partly collapsed chain. By increasing the degree of ionization, they found evidence for a conformational transition at a degree of ionization close to 0.2. Evidence was extracted from the interference peak that is characteristic for polyelectrolyte solutions with low amounts of an inert salt. Although this peak stems from interparticle interferences, its location is affected by the intraparticular form factor in a characteristic way. Addition of copper shifted this conformational transition to larger degrees of ionization.[42] Obviously, copper ions also strongly bound to the carboxylate groups, thereby neutralizing the charges. As inferred from the larger extent of shrinking, this neutralizing effect seems to be more pronounced than the one induced from protons.[42,44] At almost the same time, Sabbagh et al.[43] performed various small-angle scattering experiments. Except for a single SANS measurement, they focused on anomalous small-angle X-ray scattering (ASAXS) experiments with NaPA in the presence of bivalent metal cations close to the precipitation threshold. As a major result, they could show that the shape of the shrinking chains is reflected by the distribution of Co^{2+} ions. Yet, scattering curves from chains even in their most compact shape did not reveal a collapse but a power law of q^{-2}, indicating unperturbed dimensions only. This could be either due to the low molar mass samples used by the authors or due to the fact that they still did not get close enough to the phase boundary. Thus, all small-angle scattering experiments[40,42,44] on polyelectrolytes in the presence of multivalent cations indicate a condensation of segments more intense than induced by inert salts. However, they can hardly be interpreted in terms of a characteristic collapse toward compact structures with sharp boundaries.

At this point, we draw attention to a powerful method to gradually approach phase boundaries of L-type precipitation of polyelectrolytes[17,45] in a highly systematic way. The method was applied to the system composed of NaPA and alkaline earth cations in aqueous solutions of an inert salt. Small portions of the alkaline earth cations were introduced by replacing Na^+ ions. To isolate the specific effect of the bivalent cations from electrostatic screening effects, replacement was performed at a constant concentration of cationic charges. The phase boundary was approached by increasing the ratio of M^{2+}/COO^-. Combined static and dynamic light scattering (LS) along these approaches identified a variety of structural intermediates. They become increasingly shrunken but reached a sphere-like shape only at the very edge of the threshold.[17,45] All intermediate structures lie extremely close to the phase boundary and in preceding investigations either had not become accessible at all[40,42,43,46] or were recorded as instable intermediates only.[47]

Motivated by these achievements, we have designed SANS experiments that are suitable to investigate the shrinking mechanism of large polyelectrolyte chains in dilue solutions. The shrinking process was induced by Ca^{2+} ions in fully deuterated (D_2O) aqueous 0.01 M NaCl, corresponding to a typical L-type precipitation.

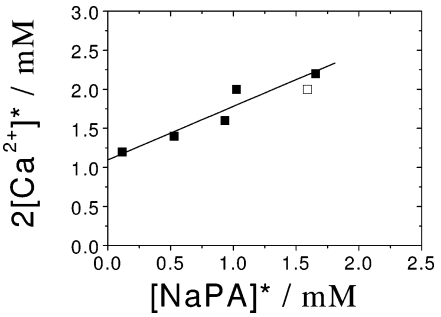

Figure 1. Phase boundary for sample PA1 in aqueous 0.01 M NaCl: (■) data from ref 45, collected in H_2O; (□) data in D_2O. The one-phase regime corresponding to a dilute transparent NaPA solution lies below the line, which is a linear fit to the data.

The relevant phase boundary to be approached is shown in Figure 1. The closed symbols denote the phase boundary obtained by LS with saline water as a solvent, whereas the open square belongs to the corresponding phase transition with saline D_2O as a solvent. An important step was to select proper solutions for SANS experiments. They should cover the most relevant regime of shrinking, providing a series of instructive intermediate structures and are most likely to be found along approaches to the phase boundary. Although being close to the phase boundary, the solutions were also required to be stable. These requirements were guaranteed by characterizing a series of solutions by LS prior to (and after) SANS experiments.

To appropriately investigate the shrinking mechanism by LS and SANS, NaPA samples with a large coil size are highly desirable: First, LS results on particle dimensions are much more significant if the polyelectrolyte particles are larger than 10 nm; second, intermediates with a pearl necklace-like shape are expected to occur only if the chains are not too short. Unfortunately, a large coil size leads to small overlap concentrations. Therefore, extremely low polymer concentrations close to 2.5×10^{-3} mol of monomers per liter had to be used to prevent the PA chains from aggregating or precipitating. This, in turn, led to a drastic decrease of the scattering signal. The situation was even worsened by the low number of H atoms per monomeric unit. As a consequence, long beam times for each solution became necessary.

Results of this combined LS and SANS investigation will be outlined in the present paper. In the second chapter, scattering experiments are described in detail. In the third chapter, the results of LS experiments will be summarized and used to select appropriate solutions for SANS experiments. Proper selection to a large extent determines the success of SANS experiments. Results from SANS will be represented and discussed in the fourth chapter. This chapter also includes a detailed comparison of experimental curves with theoretically calculated model curves. As a final result, we are able to suggest a conclusive structural model for the selected intermediates.

Experiments and Data Evaluation

Polymer Sample. The polymer sample used for the present light and neutron scattering experiments was a sodium polyacrylate sample from Polysciences (Eppelheim, Germany) with a molar mass of $M_w = 950\,000$ g/mol. On the basis of dynamic light scattering,[48] a ratio of the weight averaged (M_w) over the number averaged molar mass (M_n) was estimated to $M_w/M_n = 1.2$. The sample is denoted as PA1 and was also used in two preceding papers.[45,48]

Light Scattering. Prior to SANS experiments, detailed static and dynamic light scattering measurements were performed to select appropriate samples for SANS. The solvent was always composed of 8 mM NaCl and 1 mM $CaCl_2$ in D_2O. The deuterated water was purchased from Deutero GmbH (Kastellaun, Germany) and used without further purification. The pH was set to 9 with deuterated sodium hydroxide. The solvent used was prepared as in ref 45, the only difference is the use of deuterated water and of dry $CaCl_2$ (from Sigma-Aldrich). Then a stock solution of NaPA was prepared and gently rotated at room temperature for 5 days. The phase boundary was always approached at constant $CaCl_2$ concentration of 1 mM by varying the polymer concentration.[45]

It has to be noted that each solution has a different NaPA concentration and a different ratio of $[Ca^{2+}]$/[NaPA]. Due to the fact that the degree of complex formation between PA and Ca^{2+} depends on $[Ca^{2+}]$/[NaPA], each solution contains a different polymer species. Therefore it is not possible to extrapolate the scattering curves from static light scattering (SLS) to zero NaPA concentration. Extrapolation of the scattering data to zero scattering angle results in an apparent molecular weight M_w and an apparent radius of gyration R_g and was performed according to

$$\frac{Kc}{\Delta R_\theta} = \frac{1}{M_w} + \frac{R_g^2}{3M_w}q^2 \tag{1}$$

In eq 1 ΔR_θ is the net scattering intensity of the polymer expressed in terms of the Rayleigh ratio, K is the contrast factor of the system NaPA in 0.01 M aqueous NaCl,[45] c is the NaPA concentration in g/mL, and q is the scattering vector

$$q = (4\pi n/\lambda_0)\sin(\theta/2) \tag{2}$$

with $n = 1.329$ the refractive index of 0.01 M NaCl in D_2O, λ_0 the laser wavelength in a vacuum, and θ the scattering angle.

The results from the simultaneously recorded dynamic light scattering (DLS) was evaluated according to

$$D(q) = D_z(1 + CR_g^2q^2) \tag{3}$$

in close analogy to the SLS results. In eq 3, $D(q)$ is the angular dependent diffusion coefficient and C a dimensionless constant, sensitive to the shape of moving particles. $D(q)$ was evaluated from the correlation functions by means of the cumulant method[49] including linear and quadratic powers of the correlation time t. The extrapolated diffusion coefficient D_z was transformed into a hydrodynamically effective radius R_h according to the Stokes−Einstein equation

$$R_h = \frac{k_BT}{6\pi\eta}\cdot\frac{1}{D_z} \tag{4}$$

with k_B the Boltzmann constant, $\eta = 1133.62$ μPs the solvent viscosity of 0.01 M NaCl in D_2O, and T the absolute temperature.

Table 1. Molecular Parameters of PA1 with M_w = 950 000 g/mol in the Samples, Selected for SANS Experiments

sample	beam time	R_g/ nm	R_h/ nm	r	α_S	[NaPA]/ mM	[Ca^{2+}]/ [NaPA]
SANS-1	4. 2000	21.6	10.9	1.98	0.43	2.48	0.40
SANS-2	3. 2002	21	12.9	1.63	0.42	2.37	0.422
SANS-3	3. 2002	20.8	14.3	1.45	0.416	2.44	0.410
SANS-4	3. 2002	26.7	17.1	1.56	0.534	2.51	0.399

At the phase boundary, aggregation and precipitation competes with the intramolecular process of coil shrinking. As the focus lies on single chain form factors, solutions selected for SANS must be free of aggregation. Therefore, combined LS was performed to sort out samples that showed aggregation.[45] Two criteria were used: If the apparent particle mass determined by SLS was significantly larger than the molecular weight of the NaPA sample, aggregation has occurred. Supplementary, each DLS measurement was evaluated according to the CONTIN method.[50] CONTIN allows us to distinguish different diffusive modes. Occurrence of more than one diffusive mode was considered to be an indication for aggregates. All measurements where one of the two LS methods indicated aggregation were not considered for further data evaluation or SANS experiments.

Sample Preparation for SANS Measurements. The solvent was D_2O with 0.01 mol/L of cationic charges and with a concentration of $CaCl_2$ defined by

$$0.01\ \mathrm{M} = [Na^+] + 2[Ca^{2+}] \tag{5}$$

Volumes of solutions, selected for SANS measurement were divided into two halves, each half being filtered into a separate LS cell, respectively. Both cells were characterized with combined LS. Cleaned SANS cuvettes were first rinsed with the solvent. One of each pairs of LS cells was opened to fill the SANS cuvette. The second scattering cell of each pair of LS cells with solutions that were investigated by SANS was saved for a second characterization with combined SLS and DLS within 1 week after the SANS measurement. No change in the apparent molecular weight, in the apparent radius of gyration, and in the hydrodynamic radius could be observed. This indicated stability of the solutions under investigation.

Four NaPA solutions with Ca^{2+} ions were selected for SANS experiments and denoted as SANS-1 to SANS-4. Polyion concentrations lay in the regime of 2.3 mM < [NaPA] < 2.6 mM. Characterization of the solutions are summarized in Table 1. In addition, a Ca-free solution with the same NaPA concentration as SANS-1 was measured by SANS to investigate intermolecular interferences.

Data Evaluation of SANS Measurements. Measurements were performed at the Institut Laue-Langevin (Grenoble, France). All experiments were carried out with the D11 instrument. The cells with solutions, solvent, standard, and an empty cell were placed into a sample changer thermostated to 25 °C. The standard H_2O was measured in cuvettes with a sample thickness of 1 mm, all solutions as well as the solvent were measured at a sample thickness of 5 mm. The neutrons were detected with a ^{3}He containing area detector, which is subdivided into 64 × 64 square measuring cells with a lateral resolution of 1 cm^2. The wavelength of the neutrons was 6 Å. The scattering intensity was measured at three detector−sample distances: 20 m, 5 m, and 2.5 m corresponding to a regime of the scattering vector of 2.7×10^{-3} Å^{-1} < q < 0.25 Å^{-1}.

For further data treatment (background correction), the transmissions of the samples (liquids confined in quartz cells) have to be determined from measurements of the attenuated direct beam intensity. The transmission is in general defined as the ratio of the intensity of the sample (at scattering angle zero) I_S to that of the primary beam (without any sample) I_{EB}.

$$T = \frac{I_S(q=0)}{I_{EB}(q=0)} \tag{6}$$

From the intensity distribution of the direct attenuated beam also follows the central detector coordinates. These are used for radial averaging of the scattering data under the assumption of an isotropic scattering behavior (a certain area around the beam stop is discarded from the analysis).

With the measurement of a standard water sample (1 mm thick, T = 25 °C), detector inhomogeneities are normalized. The scattering data are put on an absolute scale by using the wavelength-dependent effective differential cross section of water,[51] tabulated for the D11 ^{3}He detector ($d\Sigma/d\Omega)_{H2O}$ = 0.905 cm^{-1} for λ = 6 Å).

The differential scattering cross section per unit volume of the solutions and the solvent are separately calculated according to the following equation[52]

$$\left(\frac{d\Sigma}{d\Omega}\right)_i = \frac{(I_i - I_{Cd}) - \dfrac{T_i(1-n_i\tau)}{T_{EC}(1-n_{EC}\tau)}(I_{EC} - I_{Cd})}{(I_{H_2O} - I_{Cd}) - \dfrac{T_{H_2O}(1-n_{H_2O}\tau)}{T_{EC}(1-n_{EC}\tau)}(I_{EC} - I_{Cd})} \cdot \frac{T_{H_2O}(1-n_{H_2O}\tau)\cdot 0.1\cdot\left(\dfrac{d\Sigma}{d\Omega}\right)_{H_2O}}{T_i(1-n_i\tau)0.5} \tag{7}$$

The indices denote sample (i), standard (H_2O), empty cell (EC) and cadmium (Cd). The cadmium measurement serves to subtract the electronic background. The term $(1 - n\tau)$ takes the correction for dead time losses into account, with n being the integral count rate of each measurement and τ being the dead time.

First, the intensity of the empty cell I_{EC} was subtracted as the sample background of the sample intensity I_i. The net polymer intensity of the NaPA chains (Pol) is obtained by subtracting the scattering cross section per unit volume of the solvent (i = Sol) from the polymer solution (i = S), both determined by eq 7.

$$\left(\frac{d\Sigma}{d\Omega}\right)_{Pol} = \left(\frac{d\Sigma}{d\Omega}\right)_S - \left(\frac{d\Sigma}{d\Omega}\right)_{Sol} \tag{8}$$

The scattering cross section per unit volume of sample SANS-3 versus the scattering vector q is shown as an example in Figure 2. At high values of q, the intensity adopts a plateau value that corresponds to the incoherent scattering intensity of the H atoms of the NaPA chains. In contrast to the coherent scattering, the incoherent scattering is isotropic in all directions in space and thus contains no information about the configuration of the atoms in a macromolecule. Therefore the incoherent scattering intensity must be subtracted from the net polymer scattering curve. All NaPA solutions investigated by SANS exhibited plateaus in

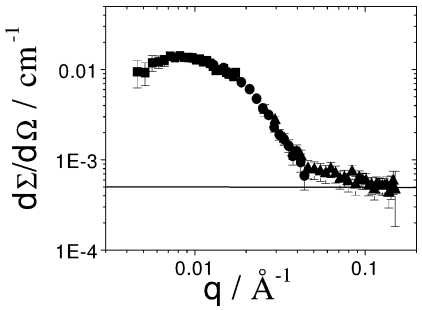

Figure 2. Scattering curve of SANS-3 evaluated according to eq 8, prior to subtraction of the incoherent background. The curve illustrates the evaluation of the corresponding incoherent scattering intensity which results from the scattering level at the largest *q*-values.

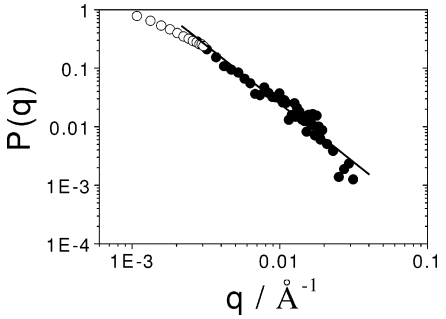

Figure 3. Scattering curve of PA1 sample in D_2O at 0.01 M NaCl without Ca^{2+}. The NaPA concentration is [NaPA] = 2.49 mM. Symbols denote LS data (○) and SANS data (●). The straight line indicates an exponent of 2.0. The SANS curve is shifted to give an overlap with the LS curve.

the scattering curves, which served to determine the corresponding incoherent background $(d\Sigma/d\Omega)_{inc}$. The final coherent net scattering intensity of the polymer $(d\Sigma/d\Omega)_{PC}$ is gained according to

$$\left(\frac{d\Sigma}{d\Omega}\right)_{PC} = \left(\frac{d\Sigma}{d\Omega}\right)_{Pol} - \left(\frac{d\Sigma}{d\Omega}\right)_{inc} \quad (9)$$

The Problem of Intermolecular Interferences. Interchain repulsion causes correlations among the chains that induces an interparticular contribution to the scattering curve. In salt-free solutions or solutions with low amounts of inert salt, these interferences even lead to a structure peak. To guarantee accessibility of reliable scattering data in terms of single chain behavior, we had to prove that the interparticular interferences were sufficiently suppressed. To this end, we first investigated the NaPA chain in deuterated water containing 0.01 M NaCl. This corresponded to the same conditions as the ones used for the measurements with Ca^{2+} cations. Although 0.01 M NaCl suppresses intramolecular interferences only in part, absence of a structure peak in this case led us to the conclusion that in all experiments carried out with divalent counterions the absence of a structure peak is even more likely because the chains are neutralized to a large extent by Ca^{2+} bonding.

Figure 3 shows the scattering curve of fully ionized NaPA in deuterated water being 0.01 M in NaCl. Due to the good solvent quality, the second osmotic virial coefficient is large, and therefore, the scattering intensity is small. The SANS data exhibit a slope close to −2, which indicates a coiled conformation of the chains.[53] No structure peak is seen. In fact, these results are compatible with the literature. According to Williams et al.[54] and to Gröhn and Antonietti[55] the screening of polymeric charges is sufficient when the ratio of [NaCl]/[NaPA] is larger than 0.33[54] or 0.22[55] respectively. In our case, this ratio is close to 4 and thus larger by an order of magnitude, suppressing an interparticular interference peak completely.

Light Scattering Results on Shrinking CaPA in D_2O

The shrinking of polymer coils results in a decrease of the radius of gyration R_g and the hydrodynamic radius R_h. If just these overall size data were available, two dimensionless parameters turned out to be specially helpful for the investigation of shape transformations along the shrinking process.[45] The first parameter α_s is the ratio of the radius of gyration of any intermediate along the approach of the phase boundary and the radius of gyration under Θ conditions representing the unperturbed chain.

$$\alpha_s = R_g/R_g(\Theta) \quad (10)$$

This ratio quantifies the extent of expansion or shrinking. The second parameter ρ compares the radius of gyration of any intermediate along the approach of the phase boundary with the corresponding hydrodynamic radius R_h.

$$\rho = R_g/R_h \quad (11)$$

The ρ ratio is expected to be highly sensitive to the shape of the shrinking coil. For expanded chains, i.e., polymers in good solvents, Akcasu and Benmouna[56] predicted a value of 1.86 and for neutral chains under Θ conditions, a significantly lower value of $\rho = 1.5$ was evaluated.[57] Finally, for spherical shapes ρ further decreases to a value of 0.78, which is significantly smaller than 1. These ρ data can be compared with recent results on NaPA in aqueous solution at varying concentrations of NaCl.[48] The results of a single high molar mass NaPA sample yielded a decrease from $\rho =$ 1.8 to $\rho = 1.48$ as [NaCl] was increased from 0.1 to 1.5M, respectively. Detailed molar mass dependent experiments at those two limiting inert salt levels revealed exponents, which indicated 0.1 M NaCl to be a good solvent and 1.5 M NaCl to be a Θ solvent. Averaged values of $\rho = 1.53$ and $\rho = 1.84$ at [NaCl] = 1.5 M and [NaCl] = 0.1 M, respectively, support this picture.

Specific interactions of Ca^{2+} ions with the carboxylate functions have to be distinguished from the regular screening effects imposed by an inert salt. As outlined in ref 45, small concentrations of Ca^{2+} already led to drastic changes in the conformation of NaPA chains. This was achieved by inserting Ca^{2+} ions at constant overall concentrations of cationic charges. LS results thereof could conveniently be discussed as ρ versus α_s. Remarkably, the trend in the plot of ρ versus α_s was not affected by the molar mass of the selected NaPA sample, nor did it depend on the location where the phase boundary was approached.[45] It was, however, affected by the level of inert salt. The most interesting results stemmed from investigations in 0.1 M NaCl and 0.01 M NaCl. Both NaCl solutions are good solvents for NaPA and the extent of shrinking was quite dramatic if referred to NaPA coils in corresponding solutions without Ca^{2+}. However, discussion of data was confined to an extent of shrinking that led to radii smaller than the unperturbed dimensions and the respective shrink-

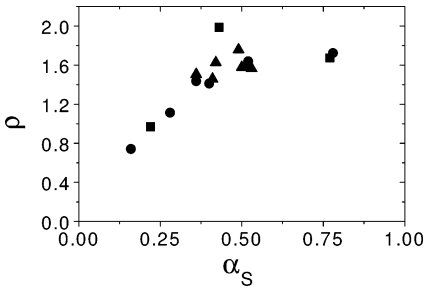

Figure 4. Representation of ρ versus α_s for PA1 in solution with 0.008 M NaCl and 0.001 M $CaCl_2$ in D_2O for three different measurement series approaching the phase boundary. The symbols refer to the following series: 04.2000 (■); 08.2001 (●); 03.2002 (▲).

ing ratios were based on the unperturbed dimensions.[45] In 0.1 M NaCl the ρ values gradually decreased from 1.6 to 0.8 as the extent of shrinking decreased from $\alpha_s = 0.75$ to $\alpha_s = 0.25$. If the NaCl level was lowered by an order of magnitude, the decrease in ρ was rather abrupt. For α_s above 0.4, ρ kept close to 1.6. Only when the shrinking ratios α_s dropped below 0.4 was the limiting value of 0.8 approached in a steep descent. This unexpected trend led us to perform SANS experiments in 0.01 M NaCl. It was our intention to select solutions that exhibit shrinking ratios close to the steep descent of ρ but still having nonspherical shapes.

For the present investigation, three approaches to the phase boundary of CaPA in D_2O with 0.01 mol/L of cationic charges were carried out. All approaches were performed at the same, constant Ca^{2+} concentration by decreasing the NaPA concentration, corresponding to an increase of $[Ca^{2+}]/[NaPA]$. The resulting solutions lay close to the phase boundary. Results are summarized in Figure 4 as ρ versus α_s. Obviously, all three approaches resulted in a single trend of ρ versus α_s, which agrees with earlier results[45] from the system in H_2O.

All three approaches were screened for intermediates that were expected to be highly suitable for SANS experiments. Three solutions were selected out of one approach. One more solution stemmed from a second approach. The solutions covered an expansion regime of $0.43 < \alpha_s < 0.54$. The corresponding ρ values were larger than 1.4 for all samples, indicating structures still far from having adopted a compact sphere. Although the solutions were extremely dilute, special care had to be taken to avoid aggregation or precipitation of CaPA. As outlined in the section "Sample Preparation for SANS Measurements", this was controlled by LS. In no case could a siginifcant change in particle size and mass be observed within 2 weeks by LS. LS results of all samples used for SANS experiments are summarized in Table 1.

SANS Results on Shrinking CaPA in D_2O

Independent of the nature of the applied waves, their intensity scattered by a particle can be expressed by the dimensionless form factor $P(q)$

$$P(q) = I(q)/I(q=0) \tag{12}$$

The form factor corresponds to the scattering intensity $I(q)$ as a function of the scattering vector q, normalized by the scattering intensity in the forward direction $I(q=0)$.

SANS curves have been successfully recorded from four different structural intermediates. As shown in Table 1, the respective ratios $[Ca^{2+}]/[NaPA]$ lie close to 0.4. All four solutions represent intermediates with an overall size roughly half of the unperturbed dimensions and with a nonspherical shape. The scattering curves are represented in Figure 5. A common feature of all four curves is a power law close to $P(q) \sim q^{-4}$ if $q > 0.02$ Å^{-1}. This dependence, denoted as the Porod law,[58] is typical for objects with sharp boundaries having defects smaller than q^{-1} and is an interesting result by itself. Sharp boundaries are associated with densely packed particles and thus point toward a highly collapsed state of the NaPA chains, which by far exceed the extent of shrinking achieved in preceding work.[40,42,43]

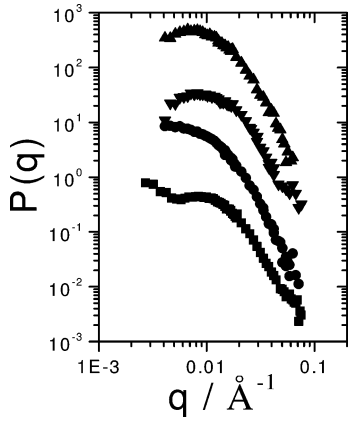

Figure 5. Scattering curves of the PA1 sample in D_2O at 0.01 M NaCl in the presence of Ca^{2+}. Symbols denote the following samples: (■) SANS-1; (●) SANS-2; (▼) SANS-3; (▲) SANS-4. The curves SANS-2, SANS-3, and SANS-4 are multiplied with appropriate factors for reasons of clearness. Characterization of the samples is summarized in Table 1.

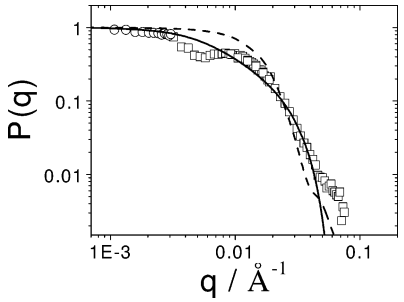

Figure 6. Scattering curve of SANS-1 in comparison to the form factor of a sphere (dashed line) and of a cylinder (solid line). Open circles denote LS data, open squares SANS data. The SANS data are shifted to give an overlap with the LS data, which are normalized to $P(q=0) = 1$. The sphere model is characterized by the following parameters: polydispersity index PDI = 1.2 and z-averaged outer sphere radius $R_h = 11$ nm. The cylinder model is characterized by a constant cross section of 13 nm, a z-averaged radius of gyration of $R_g = 22$ nm, and a polydispersity of PDI = 1.2 stemming from a distribution of the cylinder length.

The curve SANS-1 offered the chance to be normalized to $P(q=0) = 1$ because the respective SANS curve had an overlap regime in q with the corresponding light scattering curve. In Figure 6, this was achieved by simply overlaying the points within the common q regime. The corresponding shift factor may be considered to be a lower limit in an uncertainty range of 50%. The most striking feature of SANS-1, however, is the minimum at $q = 0.005$ Å^{-1}. An interparticle correlation peak as the origin of such a minimum can be ruled out if we account for the following fact. The corresponding scattering curve in 0.01 M NaCl without Ca^{2+} did not exhibit

such a peak (Figure 3). This fact makes the appearance of a peak in the presence of Ca^{2+} highly unlikely because the complexing Ca^{2+} ions significantly reduce the number of free anionic charges along the PA backbone.

Unfortunately, the low q regime of SANS-2, SANS-3, and SANS-4 did not extend as far down as it did in the case of SANS-1. Nonetheless, two of the three scattering curves, SANS-3 and SANS-4, seem to indicate a similar minimum as is observed with SANS-1. Several model objects exist that exhibit minima and maxima in their particle scattering factors. The most prominent example is a homogeneous sphere.

To apply the sphere as a potential model for our system in the first place, an appropriate size parameter has to be preselected. Fortunately, all samples were characterized by LS, which includes the determination of the z-averaged hydrodynamic radius R_h. Underlying a polydispersity index PDI = 1.2[48] with

$$\mathrm{PDI} = M_w/M_n = V_w/V_n = 1.2 \qquad (13)$$

the crucial parameter V_w is introduced. In eq 13, M_w, M_n, V_w, and V_n are the weight-averaged and number-averaged molar mass and volume, respectively. Proper values for V_w were received by varying the distribution until the averaging yields a z-averaged hydrodynamic radius equal to the one measured by DLS. Details are given in Appendix I.

Comparison of experiment with the model of a sphere is examplified in Figure 6 for the sample SANS-1. The polydispersity of PDI = 1.2 already smears the occurrence of minima in the scattering curve. As expected from the large ρ value (Table 1), the model of a sphere is not capable of describing the overall scattering curve of the sample. The size and polydispersity of the sphere model in Figure 6 was designed to be compatible with R_h from DLS. Only if $q > 0.01$ Å^{-1} is it possible to map the experimental curve with a model curve of a polydisperse sphere. However, the model sphere would only be half as large as the size of the collapsing PA chain determined by SLS.

Another possible shape for intermediates of a shrinking polyelectrolyte chain is a cigar- or saussage-like structure.[24−26,59] An adequate model for such shapes is a cylinder. In principle, the polydispersity of a cylinder depends on a variation of both the cross section and the length. We adopted a polydispersity in the cylinder length at a fixed cross section of 13 nm. This cross section was established by adjusting the scattering curve of a monodisperse cylinder to the high q regime (i.e., $q > 0.02$ Å^{-1}) of SANS-1. The length distribution was adapted to give the proper z-averaged radius of gyration from SLS and at the same time results in a PDI of 1.2. Application of this distribution to the particle scattering factor of a cylinder[60] leads to form factors of polydisperse cylinders. Two scaling regimes can be identified, a power law of $P(q) \sim q^{-1}$ typical for rod-like particles that turns into the Porod law if q is large enough. Although the form factor of a polydisperse cylinder seems to be closer to the curve SANS-1 than the model curve of the polydisperse sphere, the cylinder can just as little reproduce the minimum in the curve of Figure 6.

This led us to look for alternative models. One such model discussed for weakly charged polyelectrolyte chains in Θ solvents is the so-called trumpet.[61] The model corresponds to a chain of blobs. The size of the blobs increases toward both chain ends. However, this model is not compatible with compact objects, having a sharp boundary. Finally, the model of a pearl necklace may be the underlying shape of the collapsing chains under the present investigation. As already mentioned, this is in fact a shape suggested by numerous theoretical papers. However, in the case of a polyelectrolyte chain in a bad solvent, which collapses due to counterion condensation, Limbach and Holm[59] recently found that the regime where such structures exist is fairly narrow.

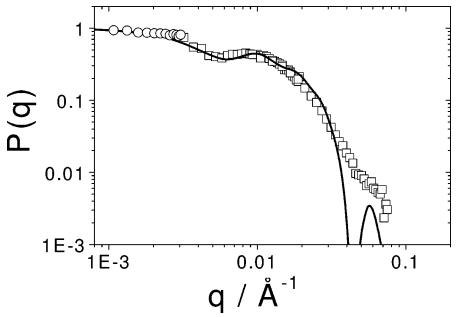

Figure 7. Scattering curve of SANS-1 in comparison to the form factor of a dumbbell. Open squares denote SANS data and open circles LS data. The SANS curve is shifted to give an overlap with the LS curve. The dumbbell is characterized by the following parameters: $A = 75$ nm, $R = 10$ nm with an R_g of 37.5 nm.

Table 2. SLS Data and Model Parameters of the Dumbbell Resulting from a Comparison of the Respective Model Curves with SANS Curves

	SLS data		dumbbell		
sample	R_g/nm	R_h/nm	R_g/nm	A/nm	R/nm
SANS-1	21.8	10.9	37.5	75	10
SANS-2[a]	21	12.9	9.3		11
SANS-3	20.8	14.3	49	100	10
SANS-4	26.7	17.1	47	100	11

[a] The theoretical parameters correspond to a polydisperse sphere with PDI = 1.2.

Meanwhile, several explicit expressions were given for model particle scattering factors of a pearl necklace chain.[21,41,62] In the most recent one,[62] a pearl necklace model was based on a freely jointed chain.[63] Rod-like segments with a fixed length are connected to a chain without bond angle restrictions, and spheres are located on each junction and at both ends of the freely jointed chain. We first compare our results with the dumbbell as the most simple structure within a homologuous series of pearl necklace chains.

In Figure 7, the same SANS curve as used in Figure 6 is compared with the scattering curve of a monodisperse dumbbell. Adjustment of the model was achieved by an extended version of the empirical relationship eq 22 of ref 62, which relates the distance A between two neighboring pearls to the q value q_{min}, where a minimum occurs in the scattering curve.

$$A = 0.89 q_{min}^{-0.87}\ (\mathrm{nm}) \qquad (14)$$

The liability of eq 14 was established for a regime of $3 < A/R < 10$. The pearl size R was estimated from the location of a shoulder, which was considered to stem from the smeared out minimum of polydisperse pearls. Model parameters for A and R are summarized in Table 2. As is shown in Figure 7, important features of the experimental curve are recovered by the model curve. However, two points have to be emphasized. (i) The dumbbell curve is based on monodiperse particles, and

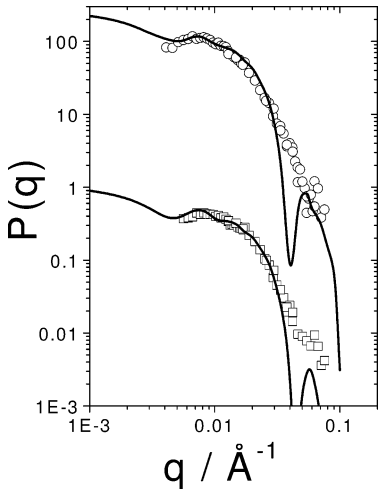

Figure 8. Scattering curve of SANS-3 (□) and SANS-4 (○) in comparison to the form factor of dumbbells. The model parameters of the dumbbells are summarized in Table 2.

sharp minima are smeared out by the polydisperse sample. (ii) The mean squared radius of gyration resulting from the dumbbell model is 37.5 nm, which is significantly larger than the experimentally determined value of $R_g = 22$ nm. We will refer to this point in a succeeding section.

Significant fractions of pearl necklace chains with more than two pearls can be excluded. The reasoning is as follows. Distances between nearest neighbors are the most frequent ones, causing the minimum in the SANS curve. If distances between two or more rod-like segments occur, they would inevitably lead to overall radii R_g even larger than 37.5 nm.

Two more scattering curves, SANS-3 and SANS-4, could be interpreted in the same way as SANS-1. Although they do not show a minimum, the existence of a maximum suffices to estimate a distance between two neighboring pearls A and the high q regime makes accessible the averaged size R of a pearl. Again, the basic features are represented by the model curve of a dumbbell, having the same drawback as in the case of SANS-1. The parameters retrieved from all three comparisons in Figures 7 and 8 are summarized in Table 2. In all cases, the pearl size is roughly $R = 10$ nm and a distance between the centers of two pearls could successfully be estimated to be 70 nm $< A <$ 100 nm. All scattering curves are dominated by the element of a dumbbell. The major discrepancy that remains to be settled is the fact that the radii of gyration measured by SLS (and SANS) were significantly smaller than the radii resulting from the dumbbell curves mapped onto the experimental curves.

The starting point for a possible resolution of this discrepancy is the likelihood for the existence of a spectrum of shapes. This is justified for several reasons. First, our NaPA sample is polydisperse. As a result thereof, a significant fraction of the chains may be too small to form two pearls in a dumbbell and collapse to single spheres. Even for monodisperse systems, Limbach and Holm[59] observed fluctuations in shape. In other words, each simulated particle adopts sphere-like, dumbbell-like, trimpbell-like shapes over certain time periods along its trajectory through time. Aside from being more realistic, a decrease of the radius of gyration is achieved if spheres are added to dumbbells. Thus, we calculated particle scattering factors for mixtures of

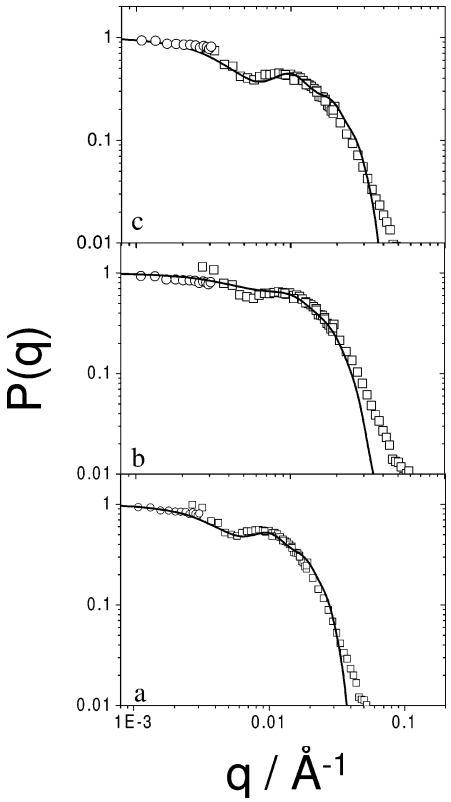

Figure 9. Scattering curve of SANS-1 in comparison to model curves: (a) mixture of the form factor of a dumbbell ($A = 75$ nm, $R = 10$ nm) and a sphere ($R = 10$ nm) with PDI = 1.11 and an averaged $R_g = 33.5$ nm; (b) mixture of the form factor of a dumbbell ($A = 75$ nm, $R = 10$ nm) and a sphere ($R = 12.7$ nm) with PDI = 1.0 and an averaged $R_g = 23$ nm; (c) pure dumbbell ($A = 75$ nm, $R = 10$ nm) with R_g of 37.5 nm. Open squares denote SANS data and open circles LS data. In Figure 9a, the SANS-1 curve is shifted by a factor of 1.25 compared to the SANS curve in Figure 9c. In Figure 9b, the SANS-1 curve is shifted by a factor of 1.45 compared to the SANS curve in Figure 9c. In Figure 9c, the SANS curve is shifted to give an overlap with the LS curve at 2.5×10^{-3} Å$^{-1} < q < 3.5 \times 10^{-3}$ Å^{-1}.

spheres and dumbbells and applied them to improve the description of SANS-1 as an example.

The mixtures of dumbbells and spheres were generated according to two alternatives: (i) The parameters A and R were adopted from Figure 7. For the sake of simplicity, the size of the single spheres were assumed to be equal to the pearl size R in the dumbbell. The advantage of this alternative is its inherent capability to account for a polydispersity of the molar mass. Above this, the location of the minimum q_{min} is expected not to be significantly affected if spheres of the same size as the pearls are added. (ii) A dumbbell with a distinct value of A and R (for the sake of simplicity we chose the same values as in alternative i) is mixed with a sphere that has the same molar mass as the dumbbell. The advantage of this alternative is that it requires a smaller amount of spheres to lower the average radius of gyration than is required in alternative i. In the light of the coarse simplifications inherent in both types of mixtures, and of the variable normalization factor for the SANS curves, we restrict ourselves to a qualitative description with theoretical examples and refrain from a quantitative fit procedure.

In Figure 9, both alternatives are compared with the interpretation based on the pure dumbbell already represented in Figure 7. Results based on alternative i

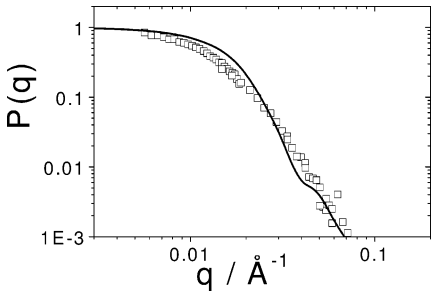

Figure 10. Scattering curve of SANS-2 (□) in comparison to the form factor of a sphere. The sphere model is characterized by the following parameters: PDI = 1.2 and *z*-averaged outer sphere radius $R = 11$ nm.

are shown in Figure 9a. In the corresponding mixture the number of dumbbells and spheres is 50% each. This composition led to the largest extent of polydispersity, $M_w/M_n = 1.11$, possible for a binary mixture of components differing in its mass by a factor of 2. Although the theoretical curve still provides a good description of the main features of SANS-1, the resulting value of R_g = 33.5 nm did not reach the experimentally determined value of $R_g = 22$ nm. Also the SANS-1 curve had to be shifted by a factor of 1.25, compared to that in Figure 9c. For the second alternative, shown in Figure 9b, a mixture of 40% dumbbells and 60% spheres was selected. This time, the radius of gyration of the generated mixture matched the value found experimentally by SLS, and with it, agreement between experiment and theory improved for $q < 3 \times 10^{-3}$ Å^{-1}. However, this improvement required a shift of the SANS-1 curve by a factor of 1.45 relative to the representation in Figure 9c. In conclusion, model mixtures of dumbbells and spheres improve representation of the overall scattering behavior of the collapsing NaPA chains, however, without achieving a complete agreement between model curves and experiment.

This scheme of dumbbell/sphere mixtures is supported by the SANS-2 scattering curve, which did not show a minimum in the experimentally accessible *q* regime. As demonstrated in Figure 10, the experimental curve can easily be fitted by the model scattering curve of a polydisperse sphere with PDI = 1.2. Again the experimentally determined radius of gyration is much larger than the value from the model curve (Table 2). Yet the scattering curve is goverened by the element of a sphere once *q* is larger than 0.007 Å^{-1}. Clearly the element of a sphere is a major constituent of the particle but does not correspond to the overall shape of the particle.

Thus, our investigation is in clear support of compact shapes for the shrinking intermediates whereas coil-like chains with a low segment density can be excluded. The best agreement among the applied models is achieved by a pearl necklace. Application of this model indicated the following features: All intermediates seem to consist of mixtures that include at least dumbbells and spheres. The distance between two pearls in the dumbbell is in the range of 75 nm < *A* < 100 nm. The pearl size is in the order of 10 nm. Although the interconnecting segment was assumed to be a rigid rod, it may well occur as a chain segment having the same conformation as a corresponding NaPA chain in 0.01 M NaCl. If we regard *A* to be close to the end-to-end distance of the interconnecting chain segment, a rough estimate of the radius of gyration would be $R_g = A/\sqrt{6}$, which corresponds to a molar mass[64] of some 200 000 g/mol. Although this oversimplifies the situation, the estimate points to a fairly large mass fraction taken up by the interconnecting string.

Conclusions

A shrinking process was induced by the introduction of specifically interacting Ca^{2+} ions. The Ca^{2+} ions bind to the carboxylate residues, neutralize the PA chain, and gradually turn the polyelectrolyte into a hydrophobic particle, insoluble in water. We have to emphasize that the origin of this polyelectrolyte coil collapse has to be distinguished from a collapse that is induced by mere counterion condensation in a solvent considered to be bad for the chain backbone.[59] In the case of specifically interacting counterions, the collapse requires stoichiometric amounts of the counterions and precedes an L-type precipitation. In the case of mere counterion condensation, a large excess of counterions, a decrease in solvent or an increase of the charge density on the chains is required to achieve coil collapse. It is usually the latter case considered by theory and simulation.

Four solutions of intermediates were selected by means of combined static and dynamic light scattering. The intermediates occurred within a shrinking process induced by Ca^{2+} ions. All four intermediates exhibited a large extent of shrinking corresponding to only 50% of the unperturbed dimensions. Yet, shape sensitive ρ values were still much closer to the coil limit than to the sphere limit.

SANS in combination with LS clearly demonstrated that all intermediates were compact particles with a sharp boundary. The scattering curves exhibited two characteristic features: (i) the obedience to the Porod law in the high *q* regime; (ii) the appearance of a maximum (and a minimum) at low *q* values, indicating an intramolecular correlation peak. From all model scattering curves compared to the SANS results, the theoretical curve of a mixture of spheres and dumbbells agreed best with the experiments. Significant contributions from larger necklace chains with more than two spheres could be excluded.

Appendix I: Particle Scattering Factor of Polydisperse Spheres and Cylinders

For polydisperse particles with a homogeneous density, the particle scattering factor is defined as

$$P(q) = \frac{\int_0^\infty w(M) M P_{\mathrm{mono}}(q)\, \mathrm{d}M}{\int_0^\infty w(M) M\, \mathrm{dM}} \qquad \text{(A1)}$$

In eq A1 $P_{\mathrm{mono}}(q)$ is the particle scattering factor of the respective monodisperse particle.

In the case of a homogeneous sphere, $P_{\mathrm{mono}}(q) = P_{\mathrm{Sp}}(q)$

$$P_{\mathrm{Sp}}(q) = \left[\frac{3}{(qR_{\mathrm{Sp}})}(\sin(qR_{\mathrm{Sp}}) - qR_{\mathrm{Sp}}\cos(qR_{\mathrm{Sp}})\right]^2 \qquad \text{(A2)}$$

with an outer radius R_{Sp}. The mass *M* of the spheres is assumed to obey a Schulz−Zimm distribution. For homogeneous spheres, the mass *M* is proportional to the volume $V = (4\pi R_{\mathrm{Sp}}^3/3)$ of a sphere and the distribution reads

$$w(V) = \frac{y^{z+1}}{\Gamma(z+1)} \cdot V^z e^{-yV} \tag{A3}$$

where

$$y = \frac{z+1}{V_w} \tag{A4}$$

and

$$\frac{V_w}{V_n} - 1 = \frac{1}{z} \tag{A5}$$

Using a value of $V_w/V_n = 1.2$ from DLS, the value of V_w is modified in an iterative procedure until the experimentally determined hydrodynamic radius could be recovered via

$$R_h = \frac{1}{\left\langle \frac{1}{R_{Sp}} \right\rangle_z} = \frac{\int_0^\infty w(V) V \, dV}{\int_0^\infty w(V) V R_{Sp}^{-1} \, dV} \tag{A6}$$

In the case of a homogeneous cylinder, $P_{mono}(q) = P_{Cy}(q)$

$$P_{Cy} = \int_0^{\pi/2} \left[\frac{2J_1(qR_{Cy} \sin x)}{qR_{Cy} \sin x} \frac{\sin[qL(\cos x)/2]}{qL(\cos x)/2} \right]^2 \sin x \, dx \tag{A7}$$

The radius of the cylinder is fixed at $R_{Cy} = 6.5$ nm. The mass M is proportional to the volume of the cylinder $V = \pi R_{Cy}^2 L$, which is varied by the length L of the cylinder.

Using a value of $V_w/V_n = 1.2$ from DLS, the value of V_w is modified in an iterative procedure until the experimentally determined radius of gyration could be recovered via

$$R_g^2 = \frac{\int_0^\infty w(V) \cdot V \cdot R_{g.mono}^2 \cdot dV}{\int_0^\infty w(V) \cdot V \cdot dV} \tag{A8}$$

Acknowledgment. Financial support of the Deutsche Forschungsgemeinschaft, Schwerpunktprogramm "Polyelektrolyte mit definierter Molekülarchitektur" SPP 1009, is gratefully acknowledged.

References and Notes

(1) Borochov, N.; Eisenberg, H. *Macromolecules* **1994**, *27*, 1440.
(2) Förster, S.; Schmidt, M.; Antonietti, M. *J. Phys. Chem.* **1992**, *96*, 4008.
(3) Flory, P. J.; Osterheld, J. E. *J. Phys. Chem.* **1954**, *58*, 653.
(4) Eisenberg, H.; Woodside, D. *J. Chem. Phys.* **1962**, *36*, 1844.
(5) Takahashi, A.; Kato, T.; Nagasawa, M. *J. Phys. Chem.* **1967**, *71*, 2001.
(6) Eisenberg, H.; Mohan, G. R. *J. Phys. Chem.* **1959**, *63*, 671.
(7) Eisenberg, H.; Casassa, E. F. *J. Polym. Sci.* **1960**, *47*, 29.
(8) Ikegami, A.; Imai, N. *J. Polym. Sci.* **1962**, *56*, 133.
(9) Wall, F. T.; Drenan, J. W. *J. Polym. Sci.* **1951**, *7*, 83.
(10) Michaeli, I. *J. Polym. Sci.* **1960**, *48*, 291.
(11) Sun, S.-T.; Nishio, I.; Swislow, G.; Tanaka, T. *J. Phys. Chem.* **1980**, *73*, 3,
(12) Meewes, M.; Ricka, J.; de Silva, M.; Nyffenegger, R.; Binkert, T. *Macromolecules* **1991**, *24*, 5811 and references therein.
(13) Wu, C.; Zhou, S. *Macromolecules* **1995**, *28*, 5388.
(14) Wu, C.; Zhou, S. *Macromolecules* **1995**, *28*, 8381.
(15) Wang, X.; Qiu, X.; Wu, C. *Macromolecules* **1998**, *31*, 2972.
(16) Chu, B.; Ying, Q.; Grosberg, A. Y. *Macromolecules* **1995**, *28*, 180.
(17) Huber, K. *J. Phys. Chem.* **1993**, *97*, 9825.
(18) Khokhlov, A. R. *J. Phys. A: Math. Gen.* **1980**, *13*, 979.
(19) Kantor, Y.; Kardar, M. *Europhys. Lett.* **1994**, *27*, 643.
(20) Kantor, Y.; Kardar, M. *Phys. Rev. E* **1995**, *51*, 1299.
(21) Dobrynin, A. V.; Rubinstein, M.; Obukhov, S. P. *Macromolecules* **1996**, *29*, 2974.
(22) Solis, F. J.; Olvera de la Cruz, M. *Macromolecules* **1998**, *31*, 5502.
(23) Micka, U.; Holm, Ch.; Kremer, K. *Langmuir* **1999**, *15*, 4033.
(24) Chodanowski, P.; Stoll, S. *J. Chem. Phys.* **1999**, *111* 6069.
(25) Schiessel, H.; Pincus, P. *Macromolecules* **1998**, *31*, 7953.
(26) Schiessel, H. *Macromolecules* **1999**, *32*, 5673.
(27) Solis, F. J.; Olvera de la Cruz, M. *J. Chem. Phys.* **2000**, *112*, 2030.
(28) Golestanian, R.; Kardar, M.; Liverpool, T. B. *Phys. Rev. Lett.* **1999**, *82*, 4456.
(29) Takagi, S.; Tsumoto, K.; Yoshikawa, K. *J. Chem. Phys.* **2001**, *114*, 6942.
(30) Lee, N.; Thirumalai, D. *Macromolecules* **2001**, *34*, 3446.
(31) Lyulin, A. V.; Dünweg, B.; Borisov, V.; Darinskii, A. A. *Macromolecules* **1999**, *32*, 3264.
(32) Kuznetsov, Yu, A.; Timoshenko, E. G.; Dawson, K. A. *J. Chem. Phys.* **1995**, *103*, 4807.
(33) Kuznetsov, Yu. A.; Timoshenko, E. G.; Dawson, K. A. *J. Chem. Phys.* **1996**, *104*, 3338.
(34) Essafi, W.; Lafuma, F.; Williams, C. E. *J. Phys. II Fr.* **1995**, *5*, 1269.
(35) Baigl, D.; Sferrazza, M.; Williams, C. E. *Europhys. Let.* **2003**, *62*, 110.
(36) Baigl, D.; Ober, D.; Qu, A.; Fery, A.; Williams, C. E. *Europhys. Lett.* **2003**, *62*, 588.
(37) Aseyev, V. O.; Klenin, S. I.; Tenhu, H.; Grillo, I.; Geissler, E. *Macromolecules* **2001**, *34*, 3706.
(38) Li, M.-J.; Green, M. M.; Morawetz, H. *Macromolecules* **2002**, *35*, 4216.
(39) Minko, S.; Kiriy, A.; Gorodyska, G.; Stamm, M. *J. Am. Chem. Soc.* **2002**, *124*, 10192.
(40) Dubois, E.; Boué, F. *Macromolecules* **2001**, *34*, 3684.
(41) Heitz, C.; Rawiso, M.; Francois, J. *Polymer* **1999**, *40*, 1637.
(42) Heitz, C.; Francois, J. *Polymer* **1999**, *40*, 3331.
(43) Sabbagh, I.; Delsanti, M.; Lesieur, P. *Eur. Phys. J. B* **1999**, *12*, 253.
(44) Ikeda, Y.; Beer, M.; Schmidt, M.; Huber, K. *Macromolecules* **1998**, *31*, 1,
(45) Schweins, R.; Huber, K. *Eur. Phys. J. E* **2001**, *5*, 117.
(46) Francois, J.; Truong, N. D.; Medjahdi, G.; Mestdagh, M. M. *Polymer* **1997**, *38*, 6115.
(47) Peng, S.; Wu, C. *Macromolecules* **1999**, *32*, 585.
(48) Schweins, R.; Hollmann, J.; Huber, K. *Polymer* **2003**, *44*, 7131.
(49) Koppel, D. E. *J. Phys. Chem.* **1972**, *57*, 4814.
(50) Provencher, S. W. *Comput. Phys.* **1982**, *27*, 213, 229.
(51) Lindner, P. *J. App. Crystallogr.* **2000**, *33*, 807.
(52) Lindner, P., Zemb, T., Eds. *Neutrons, X-rays and Light: Scattering methods applied to soft condensed matter*; Elsevier: Amsterdam, 2002; Chapter 2 (by P. Lindner).
(53) Ragnetti, M.; Oberthür, R. C. *Colloid Polym. Sci.* **1986**, *264*, 32.
(54) Williams, C. E.; Nierlich, N.; Cotton, J. P.; Jannink, G.; Boué, F.; Daoud, M.; Farnoux, B.; Picot, C.; de Gennes, P. G.; Rinaudo, M.; Moan, M.; Wolff, C. *J. Phys.* **1979**, *40*, 701.
(55) Gröhn, F.; Antonietti, M. *Macromolecules* **2000**, *33*, 5938.
(56) Akcasu, A. Z.; Benmouna, M. *Macromolecules* **1978**, *11*, 1193.
(57) Burchard, W. *Adv. Polym. Sci.* **1983**, *48*, 1.
(58) Porod, G. *Kolloid Z.* **1951**, *124*, 83.
(59) Limbach, H. J.; Holm, Ch. *J. Phys. Chem. B*, in press.
(60) Fournet, G. *Bull. Soc. Fr. Mineral. Crist.* **1951**, *74*, 39.
(61) Castelnovo, M.; Sens, P.; Joanny, J.-F. *Eur. Phys. J. E* **2000**, *1*, 115.
(62) Schweins, R.; Huber, K. *Macrom. Chem. Symp. Ser.*, in press.
(63) Hermans, J.; Hermans, J. J. *J. Phys. Chem.* **1958**, *62*, 1543.
(64) Hollmann, J. Diploma−Thesis, Paderborn, 2003.

MA0347722